Theoretical and Experimental Research of Diffraction on Round Semitransparent Ground Plane

Kirill Klionovski

***Abstract*—Round semitransparent ground plane was studied for the purpose of optimizing radiation pattern and down-up (DU) ratio of a patch antenna. This paper describes a three-dimensional diffraction of an extraneous source as a ring of magnetic current with a standing wave relative to the azimuthal coordinate on a semitransparent disk. An algorithm is given to determine the unknown electric current of the ground plane by solving the integral equation. Construction of experimental layout and method of definition of average impedance for this construction are presented. The calculated and measured radiation patterns and the DU ratio of the patch antenna with a semitransparent ground plane are compared with the conductive ground plane of the same size. The impact of the phase distribution of impedance on the DU ratio is investigated.**

***Index Terms*—Global positioning system (GPS), ground plane.**

I. Introduction

NEW applications of global navigation satellite system (GLONASS) and global positioning system (GPS) require significant improvements in users' equipment characteristics, particularly regarding radio-navigation receiver antenna. The antenna system consists of an antenna element and a ground plane, which is designed to reduce positioning errors caused by the multipath effect [1]–[4]. The effect of the multipath signal reception is characterized by the fact that the earth's surface or various objects in the vicinity of the radio-navigation receiver antenna can reflect the GLONASS/GPS signal, resulting in the signal reaching the receiver in various ways (Fig. 1). The signal reflected from the surface, as distinct from the signal transmitted directly from the satellite to the receiver, will always have a longer propagation time. The reflected signal and the direct signal are summed at the receiver with varying amplitude and phase. This leads to a positioning error.

The ability of the radio-navigation receiver antenna that is equipped with the ground plane to suppress the signal reflected from the earth or from different objects can be estimated by the down-up ratio (DU) [5]. The DU is defined as the ratio of the amplitude radiation pattern in the lower hemisphere to the amplitude radiation pattern in the upper hemisphere of the ground plane at one elevation angle θ^e (Fig. 1).

In the past few years, a significant amount of papers in the field of antennas and ground planes for global positioning systems have been published [5]–[13]. An extensive application finds the choke ring [5], [6], impedance ground planes [7], and ground planes based on thin resistive films [8].

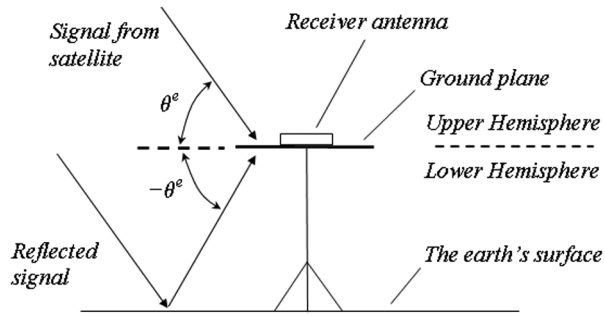

Fig. 1. Multipath effect.

One of the trends in the development of GLONASS/GPS antenna systems is the creation of ground planes, which decrease the reflected signal reception at low-elevation angles θ^e [9] (Fig. 1). This means a range of 0° to 50°. For such purposes, the use of semitransparent ground plane is possible. On the surface of such ground plane, the reflection coefficient and the transmission coefficient do not equal zero, simultaneously.

This paper describes the theoretical and experimental research carried out on round semitransparent ground plane with uneven impedance distribution on the surface of the ground planes. The phase of impedance is of an inductive character. We consider the three-dimensional diffraction of an extraneous source as a ring of magnetic current with a standing wave relative to the azimuthal coordinate on a semitransparent disk. An extraneous source in the form of a ring current with a standing wave can simulate a directional antenna, such as the patch antenna, and consider the directivity characteristics of the structure for the E-plane and the H-plane. The unknown electric current of the ground plane is determined through a numerical solution of the integral equation using the method of moments. The construction of experimental layout is described. For this construction, a method of average impedance definition is presented. The calculated and measured radiation patterns and the DU ratio of the antenna with a semitransparent ground plane at frequencies of GPS L1 (1586 MHz), GPS L2 (1236 MHz), and GPS L5 (1176 MHz) are compared with the conductive ground plane of the same size.

II. Mathematical Simulation of the Round Semitransparent Ground Plane

A. Model Structure

Figs. 2 and 3 show the model structure. At height h above the semitransparent disk of radius R is the ring of an extraneous

Manuscript received May 01, 2012; revised December 29, 2012; accepted February 09, 2013. Date of publication February 18, 2013; date of current version May 29, 2013.

The author is with the JSC Russian Space Systems, Moscow 111250, Russia (e-mail: kklionovski@mail.ru).

Color versions of one or more of the figures in this paper are available online at http://ieeexplore.ieee.org.

Digital Object Identifier 10.1109/TAP.2013.2247732

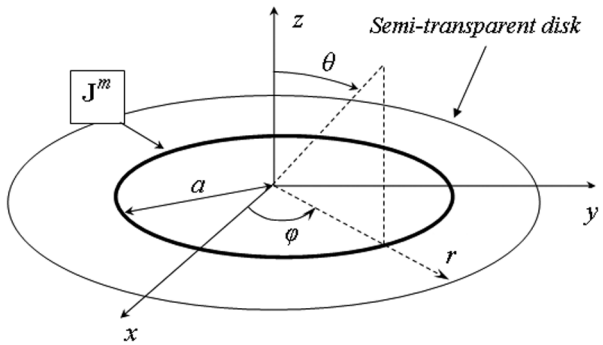

Fig. 2. Excitation of the semitransparent disk by the ring of magnetic current.

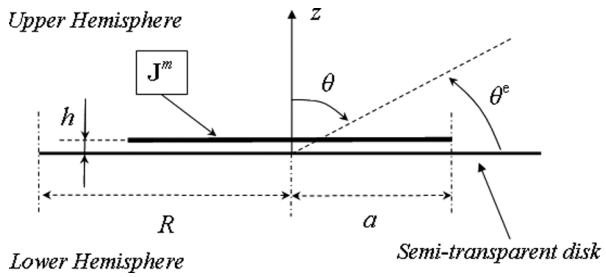

Fig. 3. Side view of the excitation of the semitransparent disk.

magnetic current with a standing wave relative to the azimuthal coordinate, radius a, and magnitude U:

$$\mathbf{J}^m = U\delta(r-a)\delta(z-h)\cos\varphi\boldsymbol{\varphi}_0. \tag{1}$$

B. Boundary Conditions

Consider the boundary conditions on the semitransparent disk [14]:

$$\mathbf{E}_\tau^+ = \mathbf{E}_\tau^-, \quad \left[\mathbf{z}_0 \times \left(\mathbf{H}_\tau^+ - \mathbf{H}_\tau^-\right)\right] = \mathbf{J}^e, \quad \mathbf{E}_\tau^+ = \hat{\mathbf{Z}}\mathbf{J}^e. \tag{2}$$

Here, $\mathbf{E}_\tau^+, \mathbf{H}_\tau^+$ are tangential components of the electric and magnetic fields on the surface of the semitransparent disk in the upper hemisphere, $\mathbf{E}_\tau^-, \mathbf{H}_\tau^-$ are tangential components of the electric and magnetic fields on the surface of the semitransparent disk in the lower hemisphere, $\mathbf{z_0}$ is the unit vector in the direction of the Z-axis, $\mathbf{J}_e$ is the electric current on disk, and $\hat{\mathbf{Z}}$ is the impedance tensor with complex components.

In the polar coordinates of the semitransparent disk (Fig. 2), the boundary conditions (2) take the form

$$\begin{aligned} E_r^+ &= E_r^- = E_r \\ E_\varphi^+ &= E_\varphi^- = E_\varphi \\ H_r^+ - H_r^- &= J_\varphi^e \\ H_\varphi^+ - H_\varphi^- &= -J_r^e. \end{aligned} \tag{3}$$

The electric current on the disk is associated with a tangential component of the electric field on the disk's surface through impedance tensor $\hat{\mathbf{Z}}$:

$$\begin{pmatrix} E_r \\ E_\varphi \end{pmatrix} = \begin{pmatrix} Z_{rr} & Z_{\varphi r} \\ Z_{r\varphi} & Z_{\varphi\varphi} \end{pmatrix} \begin{pmatrix} J_r^e \\ J_\varphi^e \end{pmatrix}. \tag{4}$$

C. Numerical Research of the Electrical Current of the Disk

Consider an integral equation of the second kind relative to the unknown electric current of the disk according to boundary condition of $\mathbf{E}_\tau^+ = \hat{\mathbf{Z}}\mathbf{J}^e$:

$$\int_{S'} \hat{\mathbf{G}}(r,\varphi,r',\varphi')\mathbf{J}^e(r',\varphi')dS' + \mathbf{E}_\tau^{ext}(r,\varphi) = \hat{\mathbf{Z}}(r)\mathbf{J}^e(r,\varphi). \tag{5}$$

Here, $\hat{\mathbf{G}}$ is the Green's tensor, $\mathbf{E}_\tau^{ext}$ is the electric field of the extraneous current in the free space, and S' is the surface of the disk. It is assumed that the elements of the impedance tensor depend only on the radial coordinate.

To numerically solve (5), the unknown electric current shall be decomposed over the basis of triangular finite elements

$$\mathbf{J}^e(r,\varphi) = \mathbf{r}_0 \sum_{n=0}^{N_r} I_n^r \Delta_r(r-r_n,\varphi) + \boldsymbol{\varphi}_0 \sum_{n=0}^{N_\varphi} I_n^\varphi \Delta_\varphi(r-r_n,\varphi). \tag{6}$$

Here, I_n^r, I_n^φ are the unknown current amplitudes, $\mathbf{r_0}$ is a radial unit vector; $\boldsymbol{\varphi_0}$ is an azimuthal unit vector, $\Delta_r(r-r_n,\varphi)$ and $\Delta_\varphi(r-r_n,\varphi)$ are the basic functions of triangular form with base $2T_r$ and $2T_\varphi$, respectively,

$$\begin{aligned} \Delta_r(r-r_n,\varphi) &= \left[1 - \frac{|r-nT_r|}{T_r}\right]\cos\varphi; \\ &\quad (n-1)T_r \le r \le (n+1)T_r \\ \Delta_\varphi(r-r_n,\varphi) &= \left[1 - \frac{|r-nT_\varphi|}{T_\varphi}\right]\sin\varphi; \\ &\quad (n-1)T_\varphi \le r \le (n+1)T_\varphi. \end{aligned} \tag{7}$$

When (5) is solved by the method of moments, a system of linear algebraic equations arises. When solving this system, the matrix of unknown current amplitudes can be determined as

$$\hat{\mathbf{I}} = (\hat{\mathbf{W}} - \hat{\mathbf{A}})^{-1}\hat{\mathbf{U}}. \tag{8}$$

The matrix elements of own and mutual impedances $\hat{\mathbf{A}}$ are calculated by numerical integration of the Green's tensor components $\hat{G}^{r(\varphi),r(\varphi)}$ and basic functions

$$\begin{aligned} A_{m,n}^{r(\varphi),r(\varphi)} &= \int_S \Delta_{r(\varphi)}(r-r_m,\varphi) \\ &\quad \cdot \int_{S'} \hat{G}^{r(\varphi),r(\varphi)}(r,\varphi,r',\varphi')\Delta_{r(\varphi)}(r'-r_n,\varphi')dS'dS. \end{aligned} \tag{9}$$

During calculation of the own, and the "nearest" mutual impedances in matrix $\hat{\mathbf{A}}$, the representation of components $\hat{G}^{r(\varphi),r(\varphi)}$ in spectral form is used. The basic function is decomposed into a two-dimensional Fourier integral over the flat sheets of the electric current. The field of such a sheet is determined by formulas [15]. Integral over the surface S' in (9) is determined by integrating the fields of flat sheets with components $\hat{G}^{r(\varphi),r(\varphi)}$.

In calculating the "distant" mutual impedances in matrix $\hat{\mathbf{A}}$, the expressions $\hat{G}^{r(\varphi),r(\varphi)}$ in the source-wise form for the ring of radial and azimuthal currents in spherical coordinates [15] are used for the purpose of reducing the computation time.

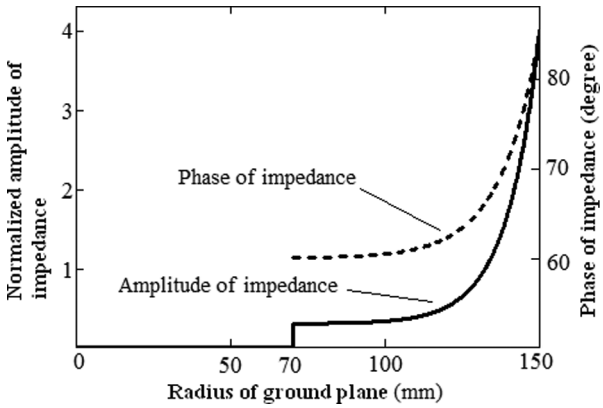

Fig. 4. Calculated impedance distribution.

The elements of matrix $\hat{\mathbf{U}}$, which describes an interaction of the extraneous source and the disk current, have the following form:

$$U_m^{r(\varphi)} = \int_S \Delta_{r(\varphi)}(r - r_m, \varphi) E_\tau^{ext}(r, \varphi) dS \qquad (10)$$

where the near-field components E^{ext} of the extraneous magnetic current in the spherical coordinates are calculated using the formulas [15].

The elements of matrix $\hat{\mathbf{W}}$ are defined as

$$W_{m,n}^{r(\varphi),r(\varphi)} = \int_S Z_{r(\varphi),r(\varphi)}(r) \Delta_{r(\varphi)}(r - r_m, \varphi) \cdot \Delta_{r(\varphi)}(r - r_n, \varphi) dS. \qquad (11)$$

The radiation pattern of the structure is determined by summing the radiation pattern of an extraneous current ring and the radiation pattern of the electric current of the disk. The far field of the ring's magnetic current in the spherical coordinates is calculated by the formulas [15]. The radiation pattern of the disk's electrical current is determined by numerical integration of the far fields from the rings of the radial and azimuthal electric currents [15]. The integration is performed over the ring's radius with amplitude distribution (6).

D. Results of Mathematical Simulation

As a result of the mathematical simulation, the impedance distribution (Fig. 4) on the surface of a semitransparent disk with a radius of 150 mm is synthesized. This provides a significant reduction in radiation in the lower hemisphere compared with a conductive ground plane of the same size at frequencies of GPS L1 (1586 MHz), GPS L2 (1236 MHz), and GPS L5 (1176 MHz). The gradient optimization method of radiation pattern is used to synthesize the impedance distribution. The impedance is equal to zero if the radius is less than 70 mm. This impedance distribution corresponds to the component Z_{rr} in the impedance tensor (4). The remaining components of (4)—$Z_{\varphi r}, Z_{r\varphi}, Z_{\varphi\varphi}$ are equal to zero. Such impedance component definition is associated with the construction of the experimental layout, which is described in Section IV. Section III provides a definition of the tensor component Z_{rr} for this construction. The components $Z_{\varphi r}, Z_{r\varphi}, Z_{\varphi\varphi}$ are assumed to be zero to simplify the solution because of the difficulty in determining them for the construction of the experimental layout. The amplitude distribution in Fig. 4 is normalized to 120π.

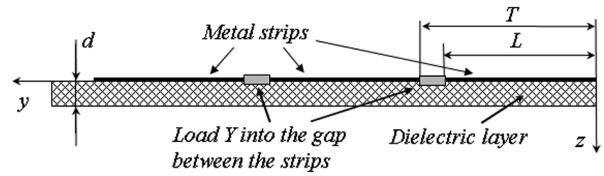

Fig. 5. Periodic structure of metal strips with a complex load in the gap.

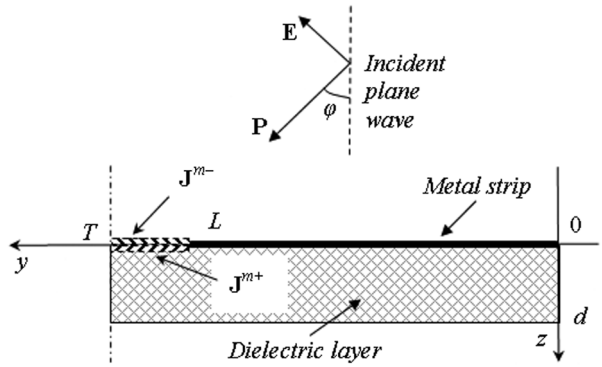

Fig. 6. Periodic cell.

III. Practical Realization of a Semitransparent Surface With an Inductive Impedance

A. Average Boundary Conditions

To gain a practical realization of the surface that can satisfy the boundary conditions (2) and provide a wide range of variations in the amplitude of impedance with the inductive phase (see Fig. 4), an array structure of metal strips that lie on the dielectric layer with a complex load in the gap between the strips can be used. The array period and the thickness of the dielectric are much smaller than the wavelength. This structure is of great interest because it can be realized easily by soldering the chip inductors and chip resistors in the gap, obtained by cutting slits in the metal layer of a foil dielectric. In researching this structure, the average impedance [14], which is determined by the values of the electromagnetic field at some distance from the surface, is of special interest.

B. Thick Array of Metal Strips on the Dielectric Layer with Complex Loads

Consider a periodic two-dimensional structure consisting of metal strips of width L and arranged with a period T (Figs. 5 and 6). In the gap between these strips, a complex load Y is included. The structure is excited by an incident plane wave at the angle φ to the OZ-axis with E-polarization. In Fig. 6, $\mathbf{P}$ is a Poynting vector and $\mathbf{E}$ is an electric field vector.

Consider a periodic cell of the structure under study (Fig. 6). To solve the task, the gap between the strips needs to be shortened and the magnetic currents $\mathbf{J}^{m+}$ and $\mathbf{J}^{m-}$ should be placed on both sides relative to the shorting plane to satisfy the boundary conditions in the gap. Because of the small size of the gap in comparison with the wavelength, we suppose that the magnetic current is constant along the entire length of the gap with complex amplitude U.

Eigenmodes of a periodic cell (Fig. 6) are determined by formulas [15]. The components of the E-wave field have the form

$$\begin{aligned}\mathbf{E}_{1m} &= \frac{\Gamma_m}{\chi_m}\mathrm{e}^{j\chi_m y}\mathrm{e}^{-j\Gamma_m z}\mathbf{y}_0 + \mathrm{e}^{j\chi_m y}\mathrm{e}^{-j\Gamma_m z}\mathbf{z}_0\\ \mathbf{H}_{1m} &= \frac{\omega\varepsilon_a}{\chi_m}\mathrm{e}^{j\chi_m y}\mathrm{e}^{-j\Gamma_m z}\mathbf{x}_0.\end{aligned} \tag{12}$$

The components of the H-wave field have the form

$$\begin{aligned}\mathbf{E}_{2m} &= \frac{\omega\mu_a}{\chi_m}\mathrm{e}^{j\chi_m y}\mathrm{e}^{-j\Gamma_m z}\mathbf{x}_0\\ \mathbf{H}_{2m} &= \frac{\Gamma_m}{\chi_m}\mathrm{e}^{j\chi_m y}\mathrm{e}^{-j\Gamma_m z}\mathbf{y}_0 + \mathrm{e}^{j\chi_m y}\mathrm{e}^{-j\Gamma_m z}\mathbf{z}_0.\end{aligned} \tag{13}$$

The longitudinal and transverse wave numbers in (12) and (13) are related by

$$\begin{aligned}\chi_m^2 &= \left(\frac{2\pi m - \varphi}{T}\right)^2\\ \Gamma_m^2 &= k^2 - \chi_m^2\\ k^2 &= \left(\frac{2\pi}{\lambda}\sqrt{\varepsilon}\right)^2\end{aligned} \tag{14}$$

where ε is the permittivity of the dielectric layer relative to free space. The components of the incident plane wave with amplitude Φ in the periodic cell are given by

$$\begin{aligned}\mathbf{E}^{inc} &= \Phi\frac{\Gamma_0}{\chi_0}\mathrm{e}^{j\chi_0 y}\mathrm{e}^{-j\Gamma_0 z}\mathbf{y}_0 + \Phi\mathrm{e}^{j\chi_0 y}\mathrm{e}^{-j\Gamma_0 z}\mathbf{z}_0\\ \mathbf{H}^{inc} &= -\Phi\frac{\omega\varepsilon_a}{\chi_0}\mathrm{e}^{j\chi_0 y}\mathrm{e}^{-j\Gamma_0 z}\mathbf{x}_0.\end{aligned} \tag{15}$$

Consider the continuity conditions of the tangential component of an electric field vector in gap $\mathbf{E}_\tau^+ = \mathbf{E}_\tau^-$. It implies that the magnetic current on both sides relative to the shorting plane (Fig. 6) is the same, with an accuracy of up to the sign

$$\mathbf{J}^{m+} = -\mathbf{J}^{m-} = \mathbf{J}^m = \begin{cases}\frac{U}{L}\mathbf{x}_0, & L < y \le T\\ 0, & 0 \le y \le L\end{cases}. \tag{16}$$

To determine the unknown amplitude U in (16), the magnetic current in a series of eigenmodes of the periodic cell needs to be decomposed:

$$\begin{aligned}\mathbf{J}^m &= [\mathbf{E}_\tau \times \mathbf{z}_0]\left[\sum_{p=1}^{2}\sum_{m=-\infty}^{\infty}\frac{c^{pm}}{L}\mathbf{E}_{pm}\times\mathbf{z}_0\right]\\ &= \begin{cases}\frac{U}{L}\mathbf{x}_0, & L < y \le T\\ 0, & 0 \le y \le L\end{cases}\end{aligned} \tag{17}$$

where $\mathbf{E}_{pm}$, components of the electric field, are determined from relations of (12) and (13). Index $\mathrm{p} = 1$ corresponds to E-waves and $\mathrm{p} = 2$ to H-waves. As far as the incident wave is the similar to the E-wave, the magnetic current $\mathbf{J}^m$ is decomposed only in the E-waves.

Applying the Lorentz lemma to expression (17), we obtain an expression of unknown decomposition coefficients c_{1m}:

$$c_{1m} = \frac{U\int\limits_{y=0}^{L} E_{1m}^* dy}{\int\limits_{y=0}^{T} E_{1m}^* E_{1m} dy} = U b_{1m}. \tag{18}$$

After the calculation of integrals in (18) by taking into account the expressions for components of eigenmodes (12), the unknown coefficients b_{1m} are determined by the following expression:

$$b_{1m} = \frac{\frac{\Gamma_m^*}{\chi_m}\frac{(\mathrm{e}^{-j\chi_m L}-1)}{-j\chi_m}}{\frac{|\Gamma_m|^2}{\chi_m^2}T}. \tag{19}$$

We define the electric current flowing through the load Y in the gap:

$$\mathbf{J}^e = Y\mathbf{E}_\tau^+ = \frac{U}{L}Y\mathbf{y}_0. \tag{20}$$

Now, we consider the continuity condition for a tangential component of the magnetic field in the gap:

$$\begin{aligned}\mathbf{H}_\tau^+ - \mathbf{H}_\tau^- &= [\mathbf{J}^e \times \mathbf{z}_0]\\ \mathbf{H}_\tau(\mathbf{J}^{m+}) - \mathbf{H}_\tau(\mathbf{J}^{m-}) - 2\mathbf{H}_\tau^{inc} &= \frac{U}{L}Y\mathbf{x}_0.\end{aligned} \tag{21}$$

The components of magnetic field $\mathbf{H}_\tau(\mathbf{J}^{m+})$ and $\mathbf{H}_\tau(\mathbf{J}^{m-}$ in (21) are defined by using their decomposition in a series of eigenmodes of a periodic cell, taking into account the reflection of the wave from the dielectric layer:

$$\begin{aligned}\mathbf{H}_\tau(\mathbf{J}^{m-}) &= -\sum_{m=-\infty}^{\infty}\frac{c_{1m}}{L}\mathbf{H}_{1m}\\ \mathbf{H}_\tau(\mathbf{J}^{m+}) &= \sum_{m=-\infty}^{\infty}\frac{c_{1m}}{L}\mathbf{H}_{1m}\left(1 + 2\frac{\rho_m^H}{1-\rho_m^H}\right).\end{aligned} \tag{22}$$

The reflection coefficient ρ_m^H of the magnetic field vector component with the index m from the dielectric layer of d thickness and a dielectric constant ε is calculated using coefficients of reflection ρ_m and transmission τ_m of the magnetic fields [15]. This is conducted for the case of inclined incidence of a plane wave with a parallel polarization to the boundary of air-dielectric $(\rho_m^{A-D}, \tau_m^{A-D})$ and dielectric-air $(\rho_m^{D-A}, \tau_m^{D-A})$:

$$\rho_m^H = \rho_m^{A-D} + \frac{e^{-j2\Gamma_m(\varepsilon)d}\tau_m^{A-D}\rho_m^{D-A}\tau_m^{D-A}}{1-\rho_m^{D-A}\rho_m^{D-A}e^{-j2\Gamma_m(\varepsilon)d}}. \tag{23}$$

Consider the equation of the power balance in the gap, which follows from (21):

$$\begin{aligned}\int\limits_{y=0}^{L}\mathbf{J}^{m^*}\mathbf{H}_\tau(\mathbf{J}^{m+})dy - \int\limits_{y=0}^{L}\mathbf{J}^{m^*}\mathbf{H}_\tau(\mathbf{J}^{m-})dy\\ - \int\limits_{y=0}^{L}\mathbf{J}^{m^*}2\mathbf{H}_\tau^{inc}dy = \int\limits_{y=0}^{L}\mathbf{J}^{m^*}\frac{U}{L}Y\mathbf{x}_0 dy.\end{aligned} \tag{24}$$

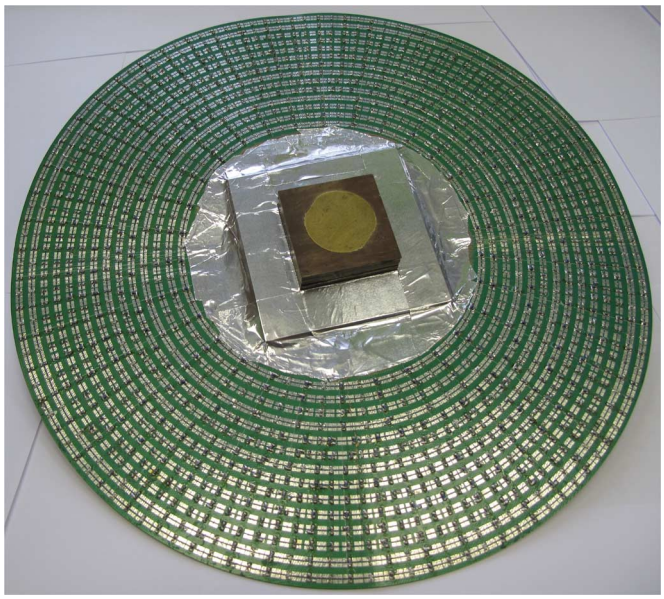

Fig. 7. Semitransparent ground plane.

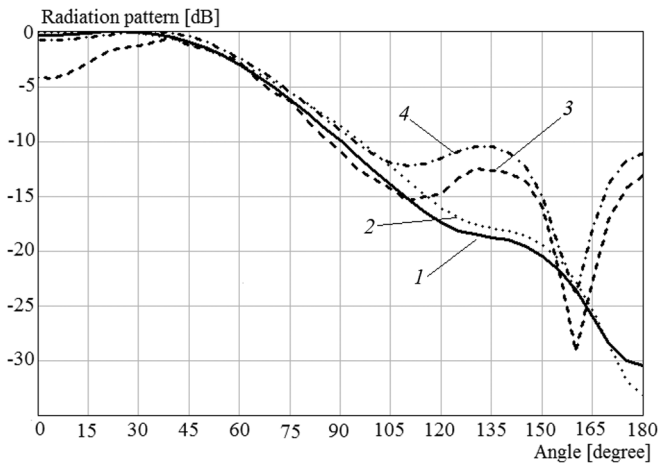

Fig. 8. Radiation pattern in the E-plane at the frequency of 1586 MHz: 1—semitransparent ground plane, measurement; 2—semitransparent ground plane, calculation; 3—conductive ground plane, measurement; and 4—conductive ground plane, calculation.

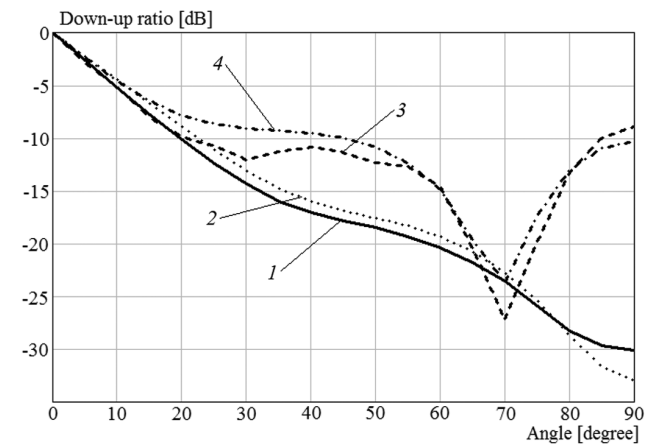

Fig. 9. Down-up ratio in the E-plane at the frequency of 1586 MHz: 1—semitransparent ground plane, measurement; 2—semitransparent ground plane, calculation; 3—conductive ground plane, measurement; and 4—conductive ground plane, calculation.

After calculating the integrals in (24), we obtain an expression for the unknown amplitude of the magnetic current in the gap:

$$U = \frac{2\frac{\Phi}{L^2}\frac{\omega\varepsilon_a}{\chi_0}\frac{(e^{j\chi_0 L}-1)}{j\chi_0}}{\sum\limits_{m=-\infty}^{\infty}\frac{b_{1m}}{L^2}\frac{1}{W_{1m}}\frac{\Gamma^m}{\chi_m}\frac{(e^{j\chi_m L}-1)}{j\chi_m}\left(2+2\frac{\rho_m^H}{1-\rho_m^H}\right)+\frac{Y}{L}}. \tag{25}$$

The reflection coefficient ρ from the structure of metal strips is calculated using the known components of the field of incident and reflected wave. To determine the average impedance of the structure, a periodic cell needs to be presented in the form of a long transmission line with the characteristic impedance W_{10} and complex impedance Z included in the section $z = 0$. The average impedance value is evaluated through the reflection coefficient using a formula from the theory of long transmission line:

$$Z = -\frac{W_{10}(1+\rho)}{2\rho} = -\frac{\frac{\Gamma_m}{\omega\varepsilon_a}(1+\rho)}{2\rho}. \tag{26}$$

IV. Results of Calculations and Experimental Research

To verify the calculated data, presented in Section II-D, layouts were made of the semitransparent and the conductive ground planes with the same diameter. The semitransparent ground plane was made in disk form with a 150-mm radius, based on a one-sided foil dielectric, with the permittivity of 3.2 and a thickness of 0.76 mm (Fig. 7).

In the metalized layer with a period of 5.8 mm along the radial direction, 14 slits of 0.5-mm thickness were cut. These slits constituted concentric circles. The minimum radius of the gap was 70 mm. On both sides of each slit, the contact pads were foreseen. The chip inductors and the chip resistors were soldered to the pads with some step along the slit. The values and period of the chip element soldering were determined by the method set forth in Section III and could be chosen from the best approximation of condition of the continuous distribution of the impedance shown in Fig. 4. The surface of the ground plane and slits, except for the pads, was covered with a protective solder mask. A patch antenna was used as an antenna element. A Russian patent for an invention [16] and a WIPO patent application [17] of the described design of a semitransparent ground plane are available.

Figs. 8–19 plot the calculated and measured radiation patterns and DU ratios of semitransparent and conductive ground planes in the E- and H-planes at three frequencies: 1586, 1236, and 1176 MHz, with a step of 5°. The angle θ is (see Figs. 2 and 3) at the plots of radiation patterns in Figs. 8, 10, 12, 14, 16, and 18, and θ^e (see Figs. 1 and 3) at the plots of DU in Figs. 9, 11, 13, 15, 17, and 19.

Calculated curves are based on mathematical model of excitation the semitransparent disk by the extraneous magnetic current ring. When calculating the radius of the extraneous current ring, a (Figs. 2 and 3) is assumed to be 50, 85, and 95 mm for frequencies 1586, 1236, and 1176 MHz, respectively. The distance between the extraneous current ring and ground plane h

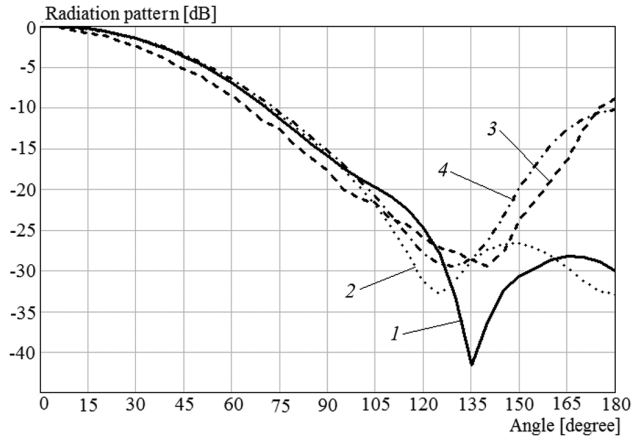

Fig. 10. Radiation pattern in the H-plane at the frequency of 1586 MHz: 1—semitransparent ground plane, measurement; 2—semitransparent ground plane, calculation; 3—conductive ground plane, measurement; and 4—conductive ground plane, calculation.

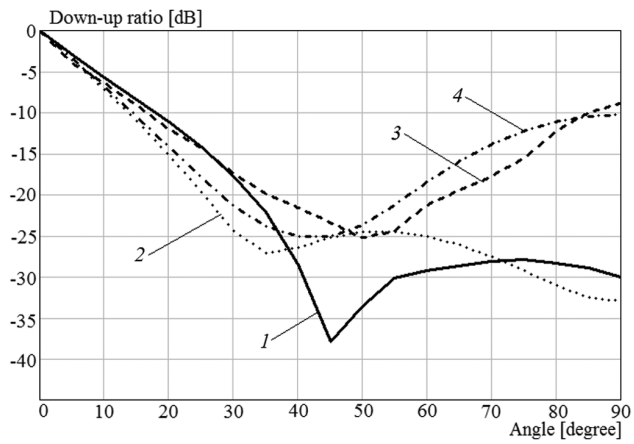

Fig. 11. Down-up ratio in the H-plane at the frequency of 1586 MHz: 1—semitransparent ground plane, measurement; 2—semitransparent ground plane, calculation; 3—conductive ground plane, measurement; and 4—conductive ground plane, calculation.

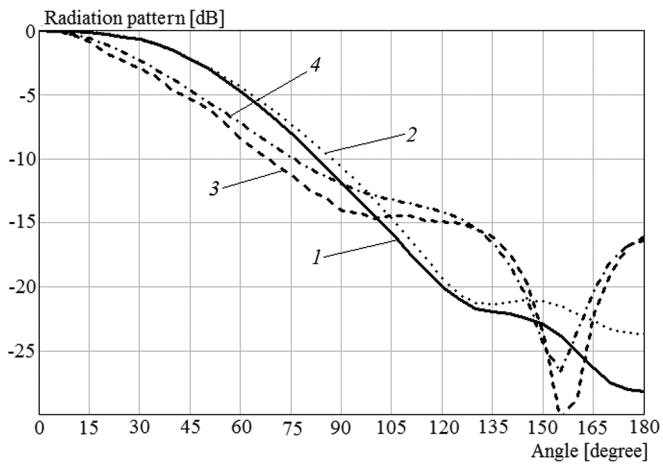

Fig. 12. Radiation pattern in the E-plane at the frequency of 1236 MHz: 1—semitransparent ground plane, measurement; 2—semitransparent ground plane, calculation; 3—conductive ground plane, measurement; and 4—conductive ground plane, calculation.

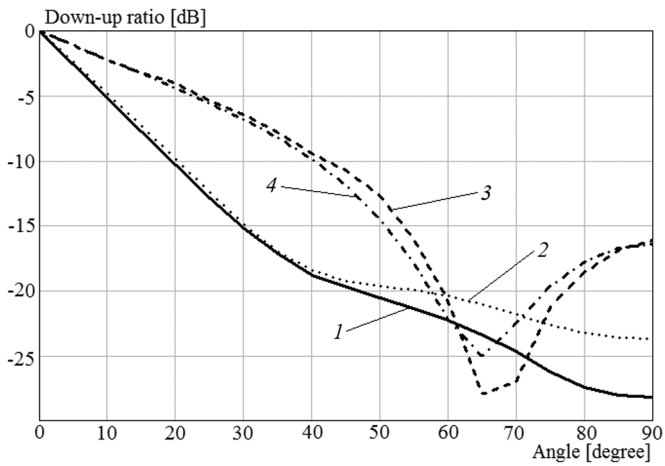

Fig. 13. Down-up ratio in the E-plane at the frequency of 1236 MHz: 1—semitransparent ground plane, measurement; 2—semitransparent ground plane, calculation; 3—conductive ground plane, measurement; and 4—conductive ground plane, calculation.

(Fig. 3) is assumed to be 1 mm. The location period of basic functions $T_{r(\varphi)}$ is equal to less than 0.025 of the wavelength.

When calculating the curves for the conducting ground plane, all the tensor components $\hat{\mathbf{Z}}$ (4) are set to zero to satisfy the boundary condition $\mathbf{E}_{\tau}^{+} = 0$ on the metal surface.

Figs. 8–19 show a good agreement between the calculated and the measured radiation patterns for the semitransparent and the conductive ground planes in the sector of angles 0°–120°. For the range of angles 120°–180°, the values of measured radiation patterns of the semitransparent ground plane are a few dB less than the values of the calculated. In general, the mathematical model describes quite well an actual radiation pattern of the patch antenna with a semitransparent ground plane.

The results considered in Section III for the two-dimensional periodic cell in Cartesian coordinates are not the same in polar coordinates, and boundary conditions of periodic cell do not take into account the impedance changing from one cell to another. However, the measured results show that average impedance (26) can be used with high accuracy for approximation calculation of impedance distribution (Fig. 4) of a round semitransparent ground plane. Moreover, good agreement between calculated and measured data is obtained under the assumption that components of the tensor (4)—$Z_{\varphi r}, Z_{r\varphi}, Z_{\varphi\varphi}$ are equal to zero.

Subsequent refinement of the model is possible by simulating the radiation pattern and the field of a real antenna in the near-field zone, as well as by a more accurate approximation of calculated impedance during the manufacture of the experimental layout.

The measured radiation pattern of the semitransparent ground plane in the E- and the H-plane at the level of 90° is one or two decibels higher than the radiation pattern of the conductive ground plane. A significant decrease in the level of a signal reflected from the earth for the semitransparent ground plane in comparison with the conductive ground plane was obtained. The decrease can be estimated according to the DU ratio. For a 90° angle in the E-plane and the H-plane, the decrease in DU is 22, 12, and 8 dB at 1586, 1236, and 1176 MHz, respectively. The decrease of DU in the E-plane for a 40° angle is 6.5, 8.5, and

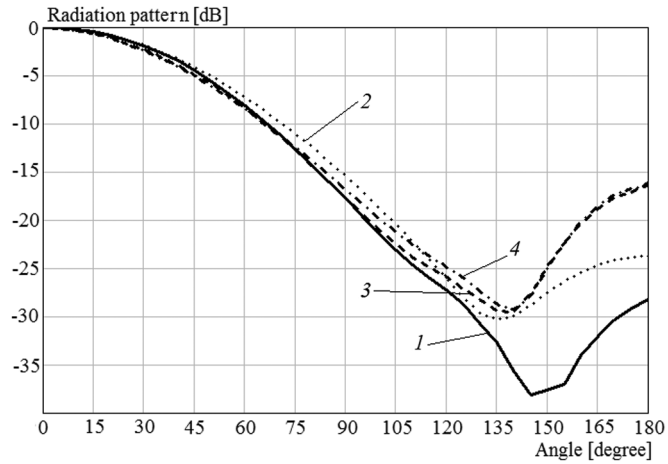

Fig. 14. Radiation pattern in the H-plane at the frequency of 1236 MHz: 1—semitransparent ground plane, measurement; 2—semitransparent ground plane, calculation; 3—conductive ground plane, measurement; and 4—conductive ground plane, calculation.

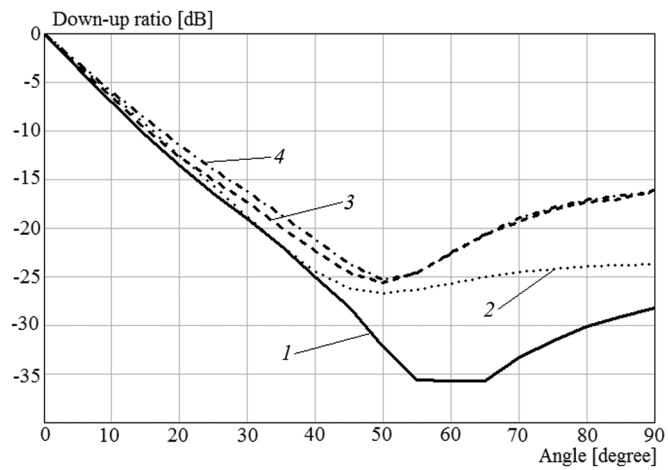

Fig. 15. Down-up ratio in the H-plane at the frequency of 1236 MHz: 1—semitransparent ground plane, measurement; 2—semitransparent ground plane, calculation; 3—conductive ground plane, measurement; and 4—conductive ground plane, calculation.

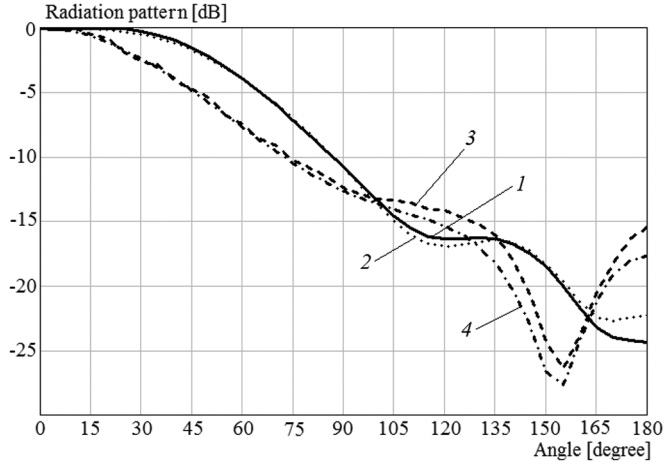

Fig. 16. Radiation pattern in the E-plane at the frequency of 1176 MHz: 1—semitransparent ground plane, measurement; 2—semitransparent ground plane, calculation; 3—conductive ground plane, measurement; and 4—conductive ground plane, calculation.

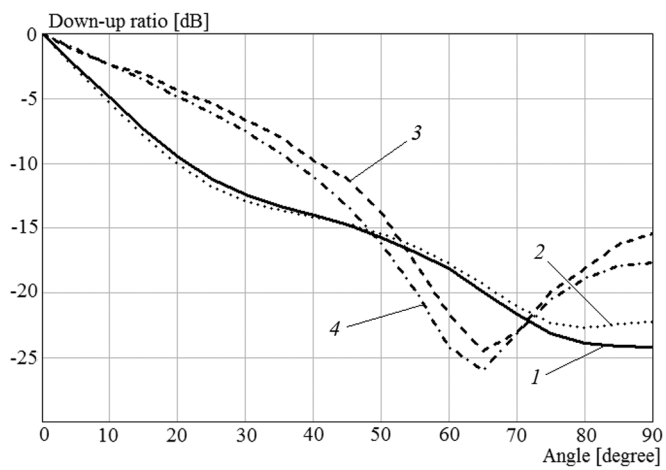

Fig. 17. Down-up ratio in the E-plane at the frequency of 1176 MHz: 1—semitransparent ground plane, measurement; 2—semitransparent ground plane, calculation; 3—conductive ground plane, measurement; and 4—conductive ground plane, calculation.

4 dB at 1586, 1236, and 1176 MHz, respectively. At 1586 MHz, the decrease of DU in the H-plane is 15 dB for a 45° angle. The decrease of DU in the H-plane is 7.5 dB at 1236 MHz for the angle of 50°. The decrease of DU in the H-plane at 1176 MHz is 18 dB for the angle of 40°.

Thus, the use of a semitransparent ground plane allows significant suppression of the reflected signal because of multipath propagation in the E- and H-planes at low-elevation angles at frequencies 1586, 1236, and 1176 MHz, compared with use of a conductive ground plane of the same size. A significant decrease of DU in the semitransparent ground plane compared with the DU of the conductive ground plane is also observed for a 90° angle.

V. Influence of Impedance Phase Distribution on the DU Ratio

To research the effect of the phase distribution of the impedance across the semitransparent ground plane surface to the DU, two additional layouts of the semitransparent ground plane, similar in design to the previously described layout (see Fig. 7), were calculated and experimentally tested. These layouts have a different phase distribution. Figs. 20 and 21 present diagrams of the calculated impedance distribution across the surface of the additional layouts with a radius of 150 mm. The gradient optimization method of radiation pattern was used to synthesize these impedance distributions. The impedance is equal to zero if the radius is less than 70 mm. The amplitude distribution in Figs. 20 and 21 is normalized to 120π.

The results of the experiments lead to the following conclusions. By increasing the value of the phase impedance from the center to the edge of the ground plane (Fig. 4), the measured characteristic of DU in the E-plane at 1586, 1236, and 1176 MHz for angles 30° and 90° varies from -13 to -15 dB and from -24 to -30 dB, respectively.

For a uniform distribution of the phases over the surface (see Fig. 20) the measured DU in the E-plane at the three frequencies for angles 30° and 90° ranging from -14 to -18 dB and from -20 to -23 dB, respectively. By decreasing the values of

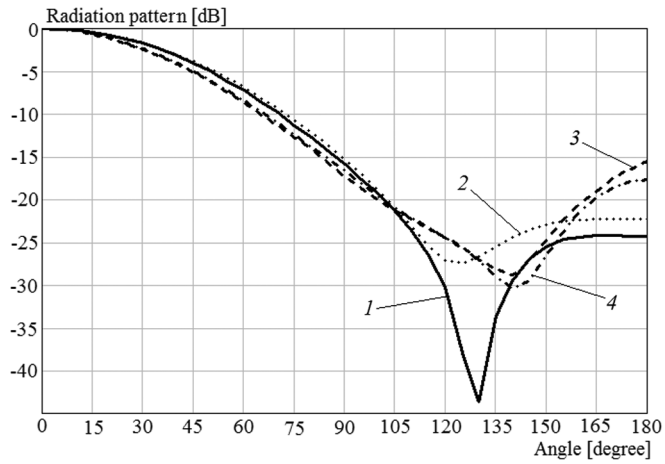

Fig. 18. Radiation pattern in the H-plane at the frequency of 1176 MHz: 1—semitransparent ground plane, measurement; 2—semitransparent ground plane, calculation; 3—conductive ground plane, measurement; and 4—conductive ground plane, calculation.

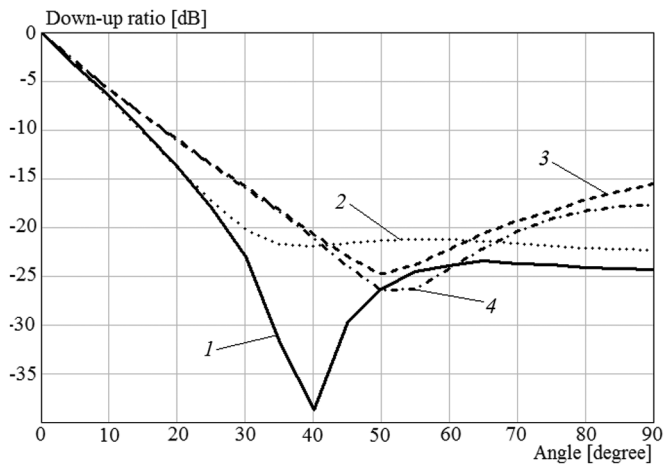

Fig. 19. Down-up ratio in the H-plane at the frequency of 1176 MHz: 1—semitransparent ground plane, measurement; 2—semitransparent ground plane, calculation; 3—conductive ground plane, measurement; and 4—conductive ground plane, calculation.

phase impedance from the center to the edge of the ground plane (Fig. 21), the measured characteristic of DU in the E-plane at the three frequencies for angles of 30° and 90° varies from -16.5 to -21 dB and from -18 to -21 dB, respectively. For the conductive ground plane, the measured DU characteristic in the E-plane at the three frequencies for angles 30° and 90° varies from -7 to -12 dB and from -9 to -16.5 dB, respectively.

Hence, it follows that by increasing the values of phase impedance from the center to the edge of the ground plane, the DU is significantly reduced for the angle of 90°. By decreasing the value of phase impedance from the center to the edge of the ground plane, the DU is significantly reduced for the angle of 30° relative to the conductive ground plane of the same size. This conclusion is valid also for DU in the H-plane. Thus, the appropriate choice of distribution of the impedance phase on the semitransparent ground plane can provide the required values of DU in the E- and H-planes for both low- and high-elevation angles.

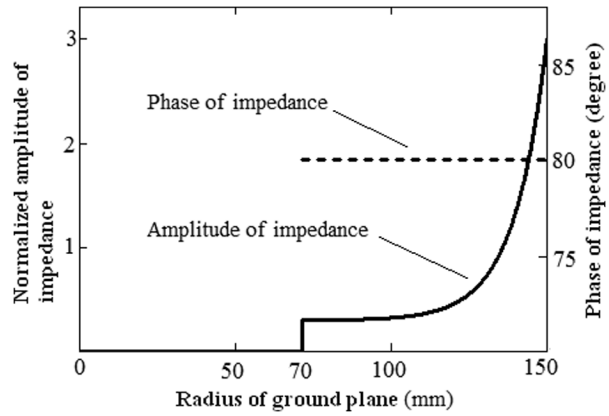

Fig. 20. Calculated impedance distribution of the first additional layout.

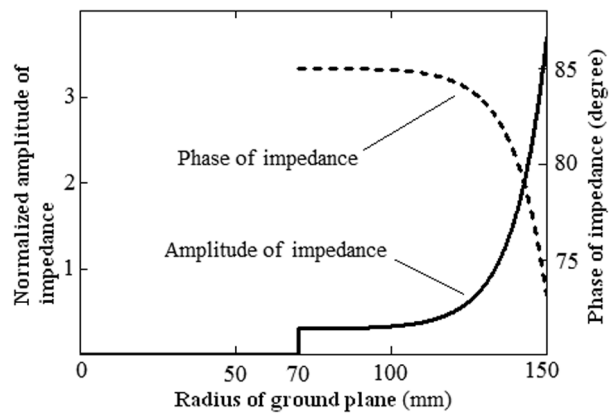

Fig. 21. Calculated impedance distribution of the second additional layout.

VI. Conclusion

We considered the task of exciting a semitransparent disk with an extraneous ring formed by a magnetic standing wave current relative to the azimuthal coordinate. A mathematical model and an algorithm for determining the current and the radiation pattern of the semitransparent ground plane in the E- and H-planes were presented. The feasibility of the practical realization of a semitransparent surface to obtain the inductive impedance was discussed.

The calculated and measured radiation patterns and DU of the round semitransparent and the conductive ground planes with a radius of 150 mm in the E- and H-planes at frequencies of 1586, 1236, and 1176 MHz were considered. The use of a semitransparent ground plane was shown to significantly suppress signals reflected because of multipath propagation in the E- and H-planes at low-elevation angles at 1586, 1236, and 1176 MHz, compared with using a conductive ground plane of the same size. A significant decrease of the DU of the semitransparent ground plane in comparison with the conductive ground plane was also observed for the angle of 90°.

We investigated the effect of the phase distribution of impedance on the DU ratio. We found that with increasing values of phase impedance from the center to the edge of the ground plane, the DU for the angle of 90° is significantly reduced. When the value of phase impedance decreases from the center to the edge of the ground plane, the DU for the angle

of 30° is significantly reduced relative to the conductive ground plane of the same size. This conclusion is also valid for the DU in the H-plane. Thus, an appropriate choice of the impedance phase distribution on the semitransparent ground plane helps to get the required values of DU in the E- and H-planes for both the low- and the high-elevation angles to the ground plane.

REFERENCES

[1] T. Kos, I. Markezic, and J. Pokrajcic, "Effects of multipath reception on GPS positioning performance," in *Proc. ELMAR Conf.*, 2010, pp. 399–402.

[2] R. Granger and S. Simpson, "An analysis of multipath mitigation techniques suitable for geodetic antennas," in *Proc. 21st Int. Technical Meeting of the Satellite Division of The Inst. of Nav. (ION GNSS '08)*, Savannah, GA, USA, 2008, pp. 2755–2765.

[3] O. Esbri-Rodriguez, M. Philipakkis, A. Konovaltsev, F. Antreich, C. Martel, and D. Moore, "Antenna-based multipath and interference mitigation for aeronautical applications: Present and future," in *Proc. 19th Int. Technical Meeting Satellite Div. of Institute of Navigation (ION GNSS 2006)*, Fort Worth, TX, USA, 2006, pp. 754–762.

[4] A. Simsky, D. Mertens, J.-M. Sleewaegen, M. Hollreiser, and M. Crisci, "Experimental results for the multipath performance of Galileo signals transmitted by GIOVE-A satellite," *Int. J. Nav. Obs.* Mar. 17, 2008 [Online]. Available: http://www.hindawi.com/journals/ijno/2008/416380

[5] Y. Lee, S. Ganguly, and R. Mittra, "Tri-band (L1, L2, L5) GPS antenna with reduced backlobes," presented at the Proc. 28th General Assembly of Int. Union of Radio Sci. (URSI-GA) New Delhi, India, 2005.

[6] F. Scire-Scappuzzo and S. N. Makarov, "A low-multipath wideband GPS antenna with cutoff or non-cutoff corrugated ground plane," *IEEE Trans. Antennas Propag.*, vol. 57, no. 1, pp. 33–46, Jan. 2009.

[7] M. Martinez-Vazquez, R. Baggen, J. Leiss, and S. Holzwarth, "Circularly polarised patch over EBG groundplane for Galileo applications," in *Proc. IEEE Antennas Propag. Soc. Int. Symp.*, 2007, pp. 4088–4091.

[8] B. Rama Rao and E. N. Rosario, "Electro-textile ground planes for multipath and interference mitigation in GNSS antennas covering 1.1 to 1.6 GHz," in *Proc. 24th Int. Tech. Meeting Satellite Div. Inst. of Nav. (ION GNSS '11)*, Portland, OR, USA, 2011, pp. 732–745.

[9] L. I. Basilio, R. L. Chen, J. T. Williams, and D. R. Jackson, "A new planar dual-band GPS antenna designed for reduced susceptibility to low-angle multipath," *IEEE Trans. Antennas Propag.*, vol. 55, no. 8, pp. 2358–2366, Aug. 2007.

[10] G. Even-Tzur and D. Shaked, "GPS antenna height and its influence on pseudorange multipath," in *Proc. FIG Working Week Conf.*, Stockholm, Sweden, 2008.

[11] M. U. Rehman, Y. Gao, X. Chen, C. G. Parini, and Z. Ying, "Analysis of GPS antenna performance in a multipath environment," in *Proc. IEEE Antennas Propag. Soc. Int. Symp.*, 2008, pp. 1–4.

[12] E. R. Gafarov and Y. P. Salomatov, "Hexagonal FSS for GLONASS/GPS antenna with improved axial ratio," in *Proc. Int. Siberian Conf. Control Commun. (SIBCON)*, 2011, pp. 159–161.

[13] M. Maqsood, S. Gao, T. Brown, and M. Unwin, "Effects of ground plane on the performance of multipath mitigating antennas for GNSS," in *Proc. Antennas Propag. Conf. (LAPC)*, Loughborough, U.K., 2010, pp. 241–244.

[14] S. Tretyakov, *Analytical Modeling in Applied Electromagnetics*. Norwood, MA, USA: Artech House, 2003.

[15] G. T. Markov and A. F. Chaplain, *Excitation of Electromagnetic Waves, [Возбуждение электромагнитных волн]*. Moscow, Russia: Radio and Communication, 1983.

[16] K. Klionovski, "Semitransparent screen for antenna of radio-navigation receiver," R.U. Patent 2,458, 439, Aug. 10, 2012.

[17] D. Tatarnikov and K. Klionovski, "Flat semi-transparent ground plane for reducing multipath," WIPO patent application WO 2011/107837, Sep. 09, 2011.

Kirill Klionovski was born in Krasnogorsk, Russia, on November 14, 1987. He received the Specialist degree (with honor) in electrical engineering from the Moscow Aviation Institute, Moscow, Russia, in 2010.

His research interests include the high-frequency diffraction and the asymptotic methods of applied electrodynamics.